Developmental Biology 222, 84–98 (2000)
doi:10.1006/dbio.2000.9709, available online at http://www.idealibrary.com on IDEAL®

Periodic Increases in Elongation Rate Precede Increases in Cytosolic Ca^{2+} during Pollen Tube Growth

Mark A. Messerli,* Robbert Créton,†,[1] Lionel F. Jaffe,† and Kenneth R. Robinson*,[2]

**Department of Biological Sciences, Purdue University, West Lafayette, Indiana 47907; and †Marine Biological Laboratory, Woods Hole, Massachusetts 02543*

Pollen tubes grown *in vitro* require an intracellular tip-high gradient of Ca^{2+} in order to elongate. Moreover, after about 2 h *in vitro* both the tip Ca^{2+} and the elongation rate of lily tubes begin to oscillate regularly with large amplitudes. This raises the question of the phase relation between these two oscillations. Previous studies lacked the temporal resolution to accurately establish this relationship. We have studied these oscillations with a newly developed, high temporal resolution system and the complementary use of both luminescent and fluorescent calcium reporters. We hereby show that the periodic increases in elongation rate during oscillatory growth of *Lilium longiflorum* pollen tubes clearly precede those in subtip calcium and do so by 4.1 ± 0.2 s out of average periods of 38.7 ± 1.8 s. Also, by collecting images of the light output of aequorin, we find that the magnitude of the $[Ca^{2+}]$ at the tip oscillates between 3 and 10 μM, which is considerably greater than that reported by fluorescent indicators. We propose an explanatory model that features cyclic growth and secretion in which growth oscillations give rise to secretion that is essential for the subsequent growth oscillation. We also critically compile data on *L. longiflorum* stylar growth rates, which show little variation from *in vitro* rates of pollen tubes grown in optimal medium.

Key Words: oscillating growth; oscillating Ca^{2+}; pollen tube; *Lilium longiflorum.*

INTRODUCTION

It is now well established that the growth of pollen tubes *in vitro* requires a cytosolic gradient of Ca^{2+}, with elevated Ca^{2+} at the growing tip (reviewed by Franklin-Tong, 1999; Miller *et al.*, 1992; Pierson *et al.*, 1994; Rathore *et al.*, 1991). If the gradient is disrupted by any means, tip growth ceases. As tip growth requires the local secretion of vesicles, it is generally assumed that the role of the Ca^{2+} gradient is to direct and regulate secretion. This is consistent with calcium's role as a near-universal regulator of secretion in other systems, including cortical vesicle fusion, neurotransmitter release (Avery *et al.*, 1999, for review), histamine release in mast cells (Baram *et al.*, 1998), and exocytosis in plant cells (Zorec and Tester, 1992). In the cases in which it has been studied with adequate temporal resolution, a triggering rise in Ca^{2+} occurs very shortly before exocytosis. For example, in the cases of neurotransmitter release and of chromaffin cell exocytosis, Ca^{2+} rises less than 60 μs (Sabatini and Regehr, 1996) and a few tens of milliseconds before exocytosis (Chow *et al.*, 1994), respectively. Thus, the discovery that pollen tube growth is not steady but oscillatory (Pierson *et al.*, 1995; Tang *et al.*, 1992) immediately raised the question of whether the tip $[Ca^{2+}]$ in pollen tubes was also oscillatory. Using a photometric system to measure light from aequorin-injected lily pollen tubes, it was found that the tip $[Ca^{2+}]$ does indeed oscillate periodically and does so with the same frequency as growth does (Messerli and Robinson, 1997). Nonratiometric imaging of Calcium Green fluorescence showed that the oscillations of $[Ca^{2+}]$ were approximately in phase with the growth oscillations, although the data suggested that the peaks of the $[Ca^{2+}]$ increase lagged the peaks of the growth rates slightly (Messerli and Robinson, 1997). Holdaway-Clarke *et al.* (1997) confirmed that lily pollen tip Ca^{2+} oscillates and

[1] Current address: OB/GYN Department, Brown University, 101 Dudley Street, Providence, RI 02905.

[2] To whom correspondence should be addressed. Fax: (765) 494-0876. E-mail: ken@video.bio.purdue.edu.

0012-1606/00 $35.00

found that these oscillations are approximately in phase with those of growth, although their data indicated that Ca^{2+} peaks a bit before growth does. However, in both cases, the resolution of the sampling method was only about 5 s, so the timing of the Ca^{2+} oscillations relative to the growth oscillations has not been adequately resolved.

Our initial efforts to achieve better temporal resolution using a laser-scanning fluorescence imaging system failed because the rapid, repeated exposure to the exciting light proved damaging to the cells. In order to reduce damage to the cells we used lower intensity light and slower scanning speeds. With this protocol, we could acquire and save images at a rate of only 0.3 Hz. We have therefore built a Ca^{2+} measuring system based upon the luminescent aequorins. It allows us to both record the light emission from aequorin-injected pollen tubes and measure growth rates with a temporal resolution of 1.5 s. Measuring Ca^{2+} dynamics with aequorin has distinct advantages over fluorescence imaging. Exciting light, which causes photodamage and limits the rate of acquisition of fluorescent images, is not needed. While cells, especially plant cells, are always autofluorescent, they are normally not autoluminescent. Also with fluorescent dyes there is a calcium-independent background, so the signal-to-background ratio is typically far better with aequorin. Also, all available dextran-linked fluorescent Ca^{2+} dyes saturate at Ca^{2+} concentrations above a few micromolar, thus limiting the upper levels of Ca^{2+} that can be measured. On the other hand, aequorin has the remarkably wide dynamic range for measuring Ca^{2+} of 0.1–100 μM (Blinks, 1989). Furthermore, aequorin is less disturbing to cell function than fluorescent dyes since aequorin has only a weak Ca^{2+} buffering capacity at cellular Ca^{2+} concentrations and is typically used at much lower concentrations within cells (Miller *et al.*, 1994).

While photometric measurements allowed us to better establish the temporal relationship of growth oscillations and Ca^{2+} oscillations, those measurements yielded little new spatial information. We have therefore used an ultra-low-light imaging device, the imaging photon detector (IPD), to visualize the distribution of Ca^{2+}-dependent aequorin luminescence in growing pollen tubes. Using fluorescence-based images to determine the basal cytosolic $[Ca^{2+}]$ in a region behind the tip and to determine the differences in the optical properties of the pollen tube tip and the zone behind the tip, we calibrated our aequorin observations and learned that the oscillating subtip $[Ca^{2+}]$ oscillates between 3 and 10 μM. These extremely high calcium levels are about three times higher than those obtained by purely fluorescent methods and yield interesting restrictions on the possible molecular receptors of the subtip calcium.

The main purpose of studying pollen tube growth *in vitro* is to better understand its growth within a flower and this approach has proven to be very fruitful at the biochemical level. However, serious uncertainties inevitably arise at the whole-system level, for which observations of isolated pollen tubes reveal only possibilities. Perhaps a good indication that similar mechanisms are controlling both *in situ* and *in vitro* growth is the maintenance of the growth rate speed. For comparison we have compiled data from the literature on lily pollen tube growth rates *in situ* and *in vitro*. This serves to show that *in vitro* rates in optimal media of *Lilium longiflorum* are practically the same as those during such stylar growth. This should add considerable significance to *in vitro* studies of the pollen tube's elongation mechanism.

MATERIALS AND METHODS

Tube Culture

L. longiflorum pollen grains were separated from the anthers, dried at room temperature for 2 days, and stored at −20°C. A small sample of pollen was hydrated in modified Dickinson's medium (in mM: 0.16 H_3BO_3, 0.127 $Ca(NO_3)_2$, 1.0 KNO_3, either 1.0 succinic acid or 5.0 MES, and 292.0 sucrose (10% w/v)), pH 5.5 with KOH. The final potassium concentration in standard medium after addition of KOH was about 2.8 mM. This pollen solution was mixed with an equal volume of 2% low-temperature-gelling agarose (FMC Co., Rockland, ME) in modified Dickinson's medium. The mixture was then put into 35 × 10-mm Falcon culture dishes with No. 1 coverglass bottoms and placed at 4°C for 1 min to gel the agarose. During photon imaging special dishes consisting of No. 0 coverglass bottoms were used. A few milliliters of modified Dickinson's medium was added to immerse the gel and the tubes were then placed in a 25°C incubator. After germination the tubes were removed from the incubator and the experiments were performed at room temperature, 20–22°C.

Photon Counting during Video Acquisition

Pollen tubes between 800 and 1000 μm in length were microinjected with a small volume of 10 mg/ml recombinant h-aequorin and placed on the microscope stage such that the tip of the tube was just showing on the left side of the video display. Photon counting was performed by collecting photons with a 40×, 1.3 NA objective on a Nikon Diaphot microscope. The photomultiplier tube (PMT) was mounted on a block that was in turn connected to the video port of the microscope. The system elements shown in Fig. 1A along with the microscope were contained in a light-tight enclosure. A cold mirror (Edmund Scientific, Barrington, NJ) was positioned in the mounting block (Fig. 1A) such that incident light between about 420 and 600 nm would be efficiently reflected to the PMT (peak emission of aequorin is 469 nm) while light with wavelengths below 420 and above 600 nm would be transmitted to the video camera. CCD cameras are very sensitive to infrared light. Two high-speed shutters were used to switch the system rapidly and repeatedly from video acquisition mode to photon counting mode. One shutter was positioned at the beginning of the transmitted light path and the other shutter was positioned immediately in front of the PMT. Figure 1B shows the collection scheme and shutter activity used during experiments. A 580-nm longpass filter was placed in the transmitted light path to reduce the intensity of light incident on the PMT shutter, which was not perfectly light tight. A second focusing element was positioned in front of the camera (Fig. 1A) to acquire a focused transmitted light image, as the primary objective was positioned immediately adjacent to the culture dish to increase the efficiency of collecting aequorin-

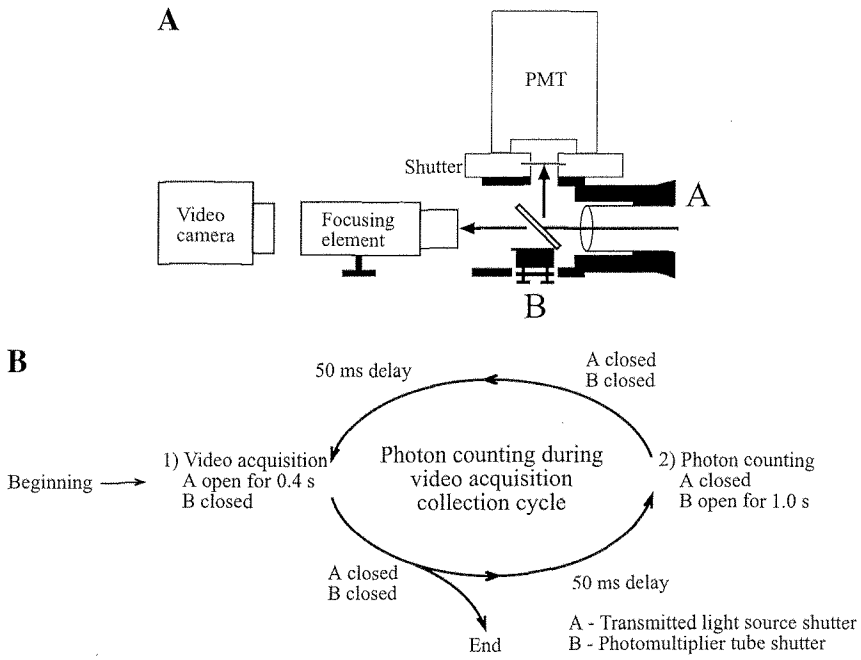

FIG. 1. (A) Diagram of the essential elements of the video/photon system. "A" indicates the side video port of the inverted Nikon Diaphot microscope. A block was machined to hold a cold mirror and fit within the video port. "B" indicates the cold mirror attached to a positioning element within the machined block. The photomultiplier tube shutter is attached directly to the block and the photomultiplier is attached directly to the shutter housing. Light collected by the objective is passed through the microscope to the video port and split by the cold mirror. Transmitted light above 580 nm passes through the cold mirror during video acquisition while aequorin-emitted light (peak emission 469 nm) is reflected to the photomultiplier tube during photon counting. (B) Data collection cycle used to collect video images intermittently with photon counting of aequorin-emitted light. The photon output recordings were aligned with the video recordings by applying a light pulse to the photomultiplier tube during the first cycle through photon counting and by noting the time stamp on the video display during the brief light pulse. The cycle was automatically repeated while the tube grew across the field of view. Termination of the cycle occurred with the acquisition of one final transmitted image. The raw data of the aequorin-emitted light were then filtered to attain only the points collected during the 1 s that the photomultiplier shutter was open.

emitted light. Our photon acquisition software was modified in order to acquire light at 0.1-s intervals and pollen tube growth rates were measured with the computer vision software described previously (Messerli *et al.*, 1999).

Photon Image Acquisition and Analysis

Imaging $[Ca^{2+}]_i$ with aequorin was performed with an imaging photon detector (Miller *et al.*, 1994). Pollen tubes between 800 and 1000 μm in length were microinjected with a small volume of 10 mg/ml recombinant h-aequorin and placed on the microscope stage such that the tip of the tube was just showing on the left side of the image photon display. Photons were acquired as the tube grew across the field of view, and the tube was repositioned after the tip grew out of the field of view. A recording consisted of imaging the light output of aequorin as the pollen tube grew across the field of view. Between 9 and 25 light output peaks and bases were collected during each recording and between 8 and 18 recordings were collected from each tube. We used a 100×, 1.3 NA objective, which resulted in a single pixel of the photon image representing approximately 1 μm^2. Figure 2 shows a flow diagram of image processing that we used in order to measure the tip $[Ca^{2+}]$ during the peaks and bases of the Ca^{2+} oscillations. We then determined the spatial distribution of the photon events by scanning the resultant arrays for the highest intensity 3 × 3-, 5 × 5-, and 10 × 10-pixel blocks at the tips of the tubes. In order to determine the tip Ca^{2+} concentration of these regions we calculated the intensity ratio of the light output from the tip regions with the light output from a region behind the growing tip. The average light output was measured for a region starting 40 μm behind the growing tip with IPDWIN95 (Science Wares, East Falmouth, MA). The average light output was collected over periods of minutes, as the light intensity behind the tip was dramatically lower. The average noise of the system was determined in a similar fashion.

Fluorescence Imaging

Pollen tubes with lengths between 800 and 1000 μm were injected with a small volume of a mixture of 2.5 mM Calcium Green dextran (10×10^3 M_r) and 5 mM Rhodamine B dextran (10×10^3 M_r) or 2.5 mM Oregon Green BAPTA-1 dextran (10×10^3 M_r) with 5 mM Rhodamine B dextran (Molecular Probes, Eugene, OR) in 100 mM KCl. Tubes were allowed to sit for approximately 1 h before imaging in order to let the dye reach the tip. Images were acquired with an MRC 1024 laser scanning confocal imaging system (Bio-Rad, Hercules, CA) connected to either an inverted

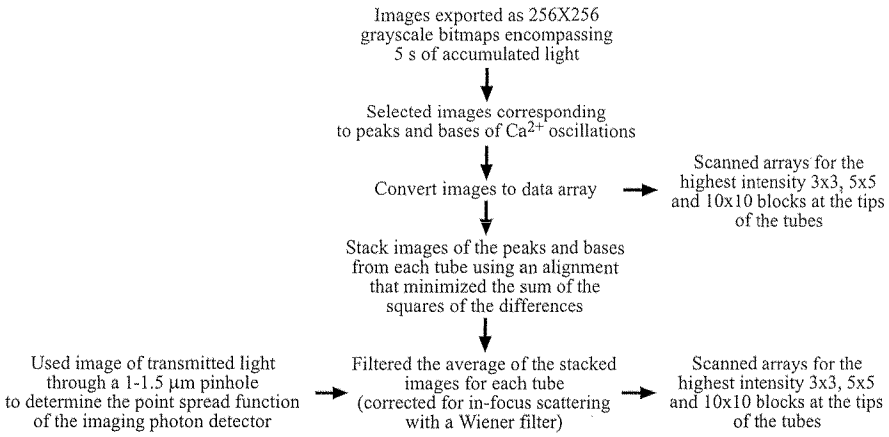

FIG. 2. Flow diagram of the image processing used to arrange and measure the low-light aequorin images. The average shifting that occurred between images during stacking was 6.2 ± 0.2 pixels, which corresponds to average tube growth rates of about 9.3 μm/min, which is very near to the growth rates previously reported (Messerli and Robinson, 1997). The signal at the base of the oscillations was too weak to perform a reliable stacking by minimizing the sum of the squares of the differences between images so we used the shifting between the peaks of the oscillations to help stack the bases of the oscillations. We always paired the base of an oscillation with the previous peak, then by knowing how much peak p shifted to best-fit peak $(p + 1)$ we had a good estimate of the shift of the tube's position between base b and base $(b + 1)$. This resulted in two arrays for each tube that reported the average pixel intensity of the peaks and the bases of the Ca^{2+} oscillations.

Nikon microscope using a 40×, 1.3 NA Nikon objective or an upright Nikon microscope using a similar objective. During imaging in the upright configuration, the culture chamber was sealed with Parafilm and inverted. The Calcium Green/Rhodamine B injectate was excited simultaneously with both 488- and 568-nm lines of the krypton/argon laser and viewed through optical filters of 522 nm with a 25-nm bandpass for the calcium indicator and 605 nm with a 35-nm bandpass for rhodamine. Both sets of images were exported and analyzed with MetaMorph imaging software (West Chester, PA). Each of the images was put through a low-pass filter before ratioing of the calcium indicator image with its corresponding Rhodamine B image. Masking of the ratioed image was used to eliminate the low background. A mask was made by selecting a pixel intensity cutoff point from the Rhodamine B image. The mask was then used to subtract out all of the background noise from around the tube. Measurements of growth rates and the relative tip-localized calcium fluorescence were then taken from the masked, ratioed images. Growth rate and tip-localized fluorescence measurements have been discussed previously (Messerli and Robinson, 1997).

The Ca^{2+} calibration was done similar to the pH calibration described earlier (Messerli and Robinson, 1998). The Ca^{2+} indicators were added to a final concentration of 10 or 20 μM with rhodamine loaded simultaneously at 20 or 40 μM. The calibration solution consisted of, in mM, 110 sucrose, 70 K^+-gluconate, 30 KOH, 10 Mops, 10 EGTA. $CaCl_2$ was added to final concentrations of 2, 3, 5.5, 7.5, 8, 9, 9.5, or 9.9 mM. Small adjustments with KOH were then used to maintain a constant pH of 7. The total concentration of all solutes was used to calculate the concentration of free Ca^{2+} in the solution with the aid of a Ca^{2+} buffer computer program. The Calcium Green curve and the Oregon Green BAPTA-1 curve were stretched to include the full 256 intensity color scale, in order to allow for a more direct comparison.

RESULTS

Photon Counting during Video Acquisition

We compared the tip-restricted $[Ca^{2+}]$ and pollen tube growth by using a high-speed shutter system that was rapidly and repeatedly switched between photon counting and the acquisition of video images from pollen tubes that were illuminated with moderate intensities of infrared light. One complete cycle lasted 1.5 s. During this (nondisturbing) method of observation, the average growth rate was 0.24 ± 0.01 μm/s. Figure 3 shows two representative recordings that were obtained in this way. It can be seen that the time of peak calcium lags that of peak growth rate in most cases. From a comparison of 243 calcium and growth oscillations in seven tubes we learned that the Ca^{2+} oscillations lagged the growth oscillations by 4.1 ± 0.2 s on average. The correlation analysis we used to determine this lag consists of a point-to-point comparison of the corresponding growth rate and tip Ca^{2+} signal waveforms. Thus the 4.1-s lag is a measurement of when the bases, peaks, rises, and falls of the two waveforms are most closely alike. The average period between oscillations during these experiments was 38.7 ± 1.8 s. The 4.1-s lag corresponds to a phase lag of 38.0 ± 1.7° out of a 360° oscillation cycle. Figure 4 shows a plot of the correlation coefficients as the Ca^{2+} oscillation recordings were shifted with respect to the growth oscillation recordings. The peak correlation for the individual tubes always occurred at either 3 or 4.5 s. The Ca^{2+} lag is statistically significant due to the fact that point

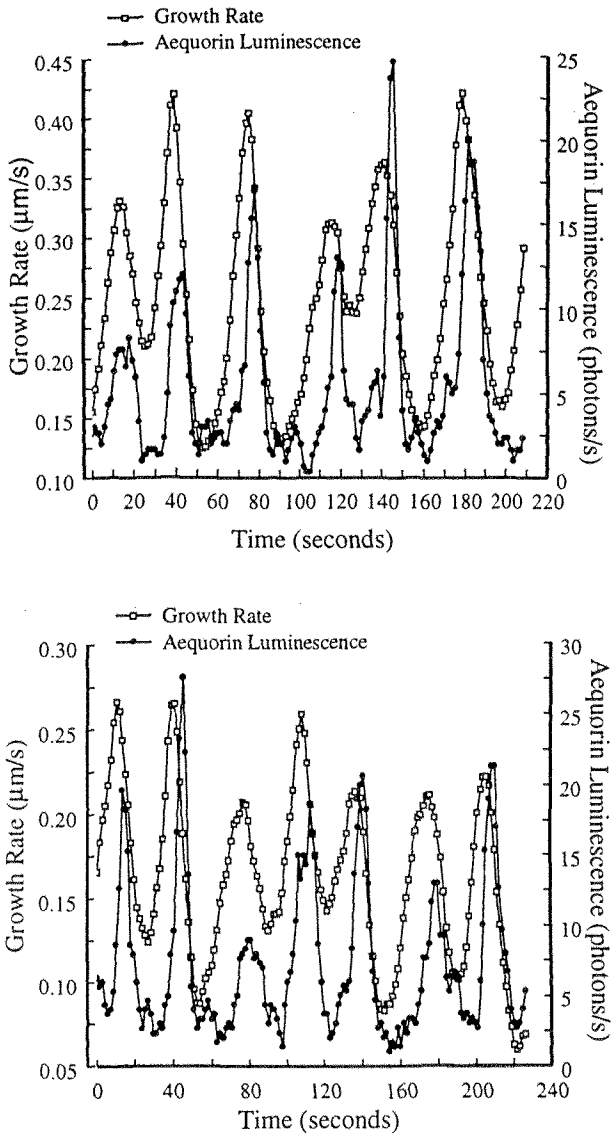

FIG. 3. Two representative line plots of the growth rates and $[Ca^{2+}]_i$ measurements collected from two different tubes with the video/photon system. Images used for growth rate calculations were collected at 1.5-s intervals. Ca^{2+} values were taken from data collected over a second and plotted in the middle of this period. It took 1.5 s to collect a video image and take a Ca^{2+} measurement. In all cases the waveforms of the Ca^{2+} oscillations lag the waveforms of the growth oscillations.

C, Fig. 4, is statistically different from points A and B (t test, $P < 0.001$ and $P < 0.03$, respectively).

Photon Imaging

Images of aequorin-injected pollen tubes were collected as they grew across the field of view by focusing their luminescence on to the photocathode of an imaging photon detector (Miller *et al.*, 1994). Figure 5A shows a line plot of the total number of photons collected for a selected region for a 10-min segment of a representative recording. The line plot marked with small circles shows the average luminescence over a large region encompassing the growth path of the tip while the unmarked plot beneath it shows the average luminescence over the rest of the image area (background). Figure 5B1 shows a raw image of the total light collected for the 4-min segment marked in Fig. 5A. The pollen tube was growing from left to right and each pixel represents approximately 1 μm^2. Figures 5B2–5B7 show raw images of 5 s of accumulated light during selected Ca^{2+} peaks (2, 4, and 6) and their subsequent bases (3, 5, and 7) of the recording shown in Fig. 5A. We measured the spatial distribution of the tip-restricted Ca^{2+} signal by determining the average number of milliphotons μm^{-2} s^{-1} for the highest intensity 3 × 3-, 5 × 5-, and 10 × 10-μm^2 regions in the raw images. The average luminescences for the 3 × 3-, 5 × 5-, and 10 × 10-μm^2 regions were 133, 96, and 58 mphotons μm^{-2} s^{-1} for the peaks, respectively, and 16, 11, and 6 mphotons μm^{-2} s^{-1} for the bases ($n = 7$). The average dark counts collected by the system were 0.08 mphotons μm^{-2} s^{-1}. For comparison we also collected the average light output of some tubes at a region 40 μm behind the growing tip and measured an average intensity of 0.17 mphotons μm^{-2} s^{-1}. We used only tubes that remained in the plane of focus for these measurements. The region behind the tip is more densely packed with organelles that

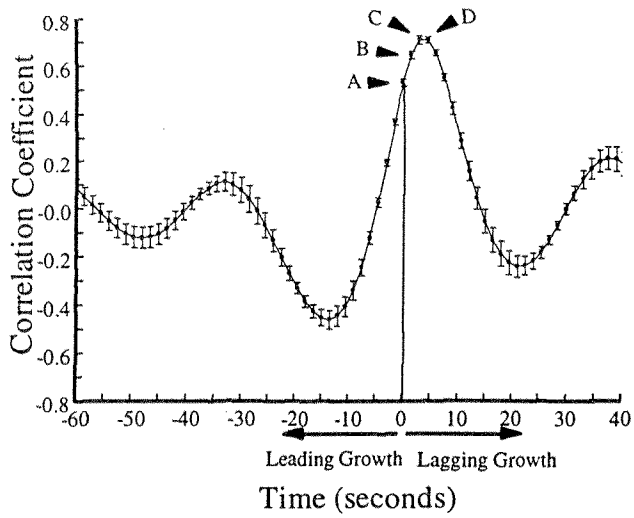

FIG. 4. Correlation analysis plot of the growth rates and Ca^{2+} measurements collected by the video/photon system. The highest correlation occurs when the Ca^{2+} oscillations lag the growth oscillations by between 3 and 4.5 s. Looking just at the absolute peaks of correlation for the individual tubes, we find that the highest correlation occurs at 4.1 ± 0.2 s. Point C is significantly different from points A and B (see text).

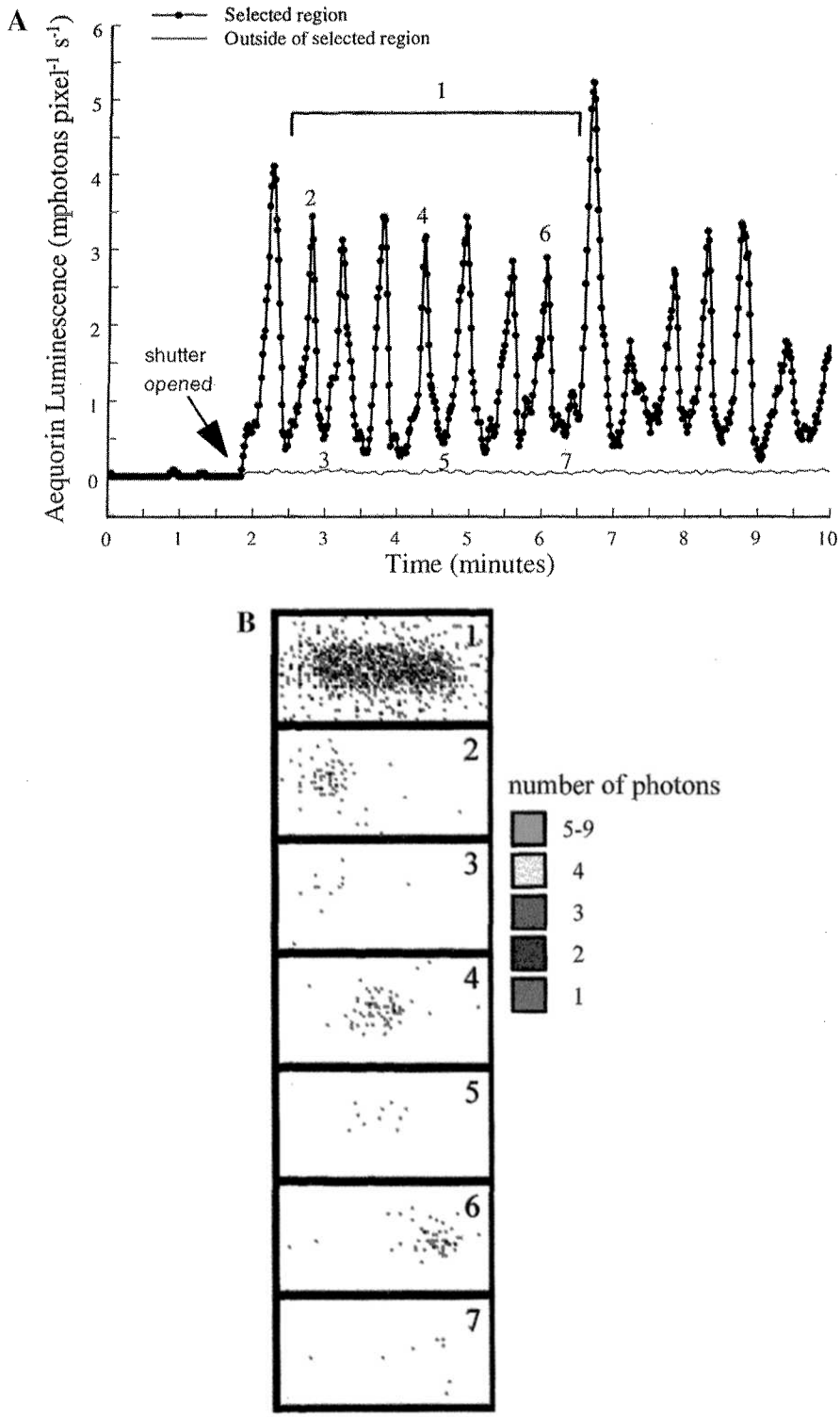

FIG. 5. Plots and images of luminescence from a representative, growing, aequorin-injected pollen tube. (A) Line plot of the luminescence collected from a region immediately surrounding the growth path of the pollen tube. This is shown as the bold line with filled circles while the thin line shows the background light collected from the region well outside of the growth path of the tube. (B1) An image formed from the photons collected during the 4-min period indicated in A. (B2–B7) Images formed from the photons collected during 5-s periods at the peaks (2, 4, and 6) and bases (3, 5, and 7) of the calcium oscillations.

tend to reduce light output. To determine the amount of light lost due to the higher density of organelles we measured the light intensity decrease of an injected fluorescent dye, Rhodamine B. We found that the fluorescent light output of Rhodamine B is on average 20% lower ($n = 6$ tubes) at a region between 40 and 70 μm behind the tip in comparison to its intensity at the tip. We assume that absorption and scattering are the same for the excitation, emission, and luminescent wavelengths, 568, 605, and 469 nm, respectively. This is a reasonable assumption, given the relatively narrow range of the relevant wavelengths and the unpigmented nature of the pollen tubes. Emitted luminescence will be reduced by only half of the ratio, 10% rather than 20%, as the organelles will equally reduce the relative intensity of both the exciting and the emitted light of fluorescent images. Applying this correction to the aequorin images we calculate that for the 3×3-, 5×5-, and 10×10-μm^2 tip-localized regions the Ca^{2+} concentration during the peaks is 34.6, 29.4, and 22.8 times greater than the region 40 μm behind the tip and 12.0, 9.9, and 7.3 times greater during the bases of the Ca^{2+} oscillations.

We used a best-fit alignment algorithm to stack and average the light signal from successive images of bases and peaks from each tube in order to visualize the average intracellular Ca^{2+} distribution during the bases and peaks of the Ca^{2+} oscillations. Figure 6A shows side profiles of the light intensity from the average of the bases (1) and peaks (2) of the Ca^{2+} oscillations of a single tube. The profiles show the intensity of light at the tip and down the shaft of the tube with the tip of the tube growing toward the right side of the figure. The x axis shows the relative distribution of the light signal. The profile of the average of the bases (1) is scattered and the leading edge of the gradient is difficult to determine. However, as the light level was so low at the bases, the best-fit algorithm could not accurately align the images. For this reason we stacked the bases of the Ca^{2+} oscillations using the shift of the preceding Ca^{2+} oscillation peak (see Materials and Methods). The profile of the average of the peaks (2), however, can be seen clearly even with the image distortion due to light scattering. Figure 6A3 shows a side view of Fig. 6A2 after correcting for imperfectly focused and scattered light (image filtering), while Fig. 6B shows a top view of Fig. 6A2 before (1) and after (2) filtering. The tips of the tubes in Fig. 6B are growing toward the right side of the figure. With deblurring we can more clearly visualize the tip-high Ca^{2+} gradient that rises steeply at the apex and drops more gradually behind the tip (Fig, 6A3). We also measure that, on average, 90% of the light output occurs in a 13 μm wide by 26 μm long region at the tip of the tube. The intensity along the shaft of the tube is a slight overestimate as the light images of the tubes had time to spread over 1.25–2 μm as the tube was growing during the 5-s accumulation period. After correcting for scattered light we found that the relative Ca^{2+} concentration at the tip compared to the region 40 μm behind the tip had risen to 42.4, 35.5, and 25.9 times greater for the peaks and 13.1, 10.7, and 7.4 times greater for the bases for the 3×3-, 5×5-, and 10×10-μm^2 regions, respectively.

Ratiometric Fluorescence Imaging

We used a ratio of Calcium Green dextran or Oregon Green BAPTA-1 dextran (Ca^{2+} sensitive) with co-injected Rhodamine B dextran (Ca^{2+} insensitive) to measure the changes in $[Ca^{2+}]_i$ while correcting for differences in light output due to the amount of dye in the light path. These tubes grew at 0.19 ± 0.01 μm/s, which is 21% slower than the 0.24 ± 0.01 μm/s value found with aequorin-injected tubes ($P < 0.02$; two-tailed t test). Thus these data are somewhat less reliable and are less accurate than our luminescence based data. Nevertheless, they do yield results that are fully consistent with and thus confirmatory of them. From calibration curves, shown in Fig. 7, it can be seen that the Calcium Green dye saturates near 2 μM and that Oregon Green saturates near 1 μM. While both dyes saturated in the low micromolar range, they were reliable at lower Ca^{2+} concentrations and allowed us to determine that the average cytosolic Ca^{2+} concentration in a region 40 μm behind the growing tip is 236 ± 8 nM ($n = 6$). We used only tubes that remained in the plane of focus for these measurements. This absolute baseline value was used to calibrate our aequorin data and thus allowed us to determine absolute Ca^{2+} levels near the tip.

Figure 8A shows a set of images collected with the dual-dye ratioing technique using Calcium Green. It can be seen that the region of the highest $[Ca^{2+}]_i$ is localized to the leading edge of growth and that during the peaks of the Ca^{2+} oscillations the $[Ca^{2+}]$ at the tip increases and the Ca^{2+} gradient extends farther down the shaft of the tube. Careful observation of the figure allows the reader to see the enhanced elongation of the tube around the time of the increased $[Ca^{2+}]$. In Fig. 8B we show the Calcium Green-measured $[Ca^{2+}]_i$ changes during growth rate changes for another tube. The $[Ca^{2+}]$ within 0.6 μm of the tip oscillated between about 0.9 and 2 μM during this recording. Also in Fig. 8B, for comparison, we show that the $[Ca^{2+}]$ for a 2×2-μm^2 region at the tip of this tube oscillates between about 0.5 and 0.9 μM. The growth rate for this tube is shown superimposed on the two $[Ca^{2+}]$ plots. It can be seen that most of the peaks of the Ca^{2+} oscillations occur after the peaks of the preceding growth oscillations. Figure 9 displays the results of the correlation analysis that was used to determine the phase relationship between the growth oscillations and the Ca^{2+} oscillations. The highest correlation occurs when the calcium oscillations lag the growth oscillations by about 2.5 s although the statistical significance of this lag is only marginal. The data from the Calcium Green- and Oregon Green-injected tubes were combined for correlation analysis (96 oscillations from five tubes). The oscillations from each tube were averaged together before analysis so that one tube did not influence the results more than another tube.

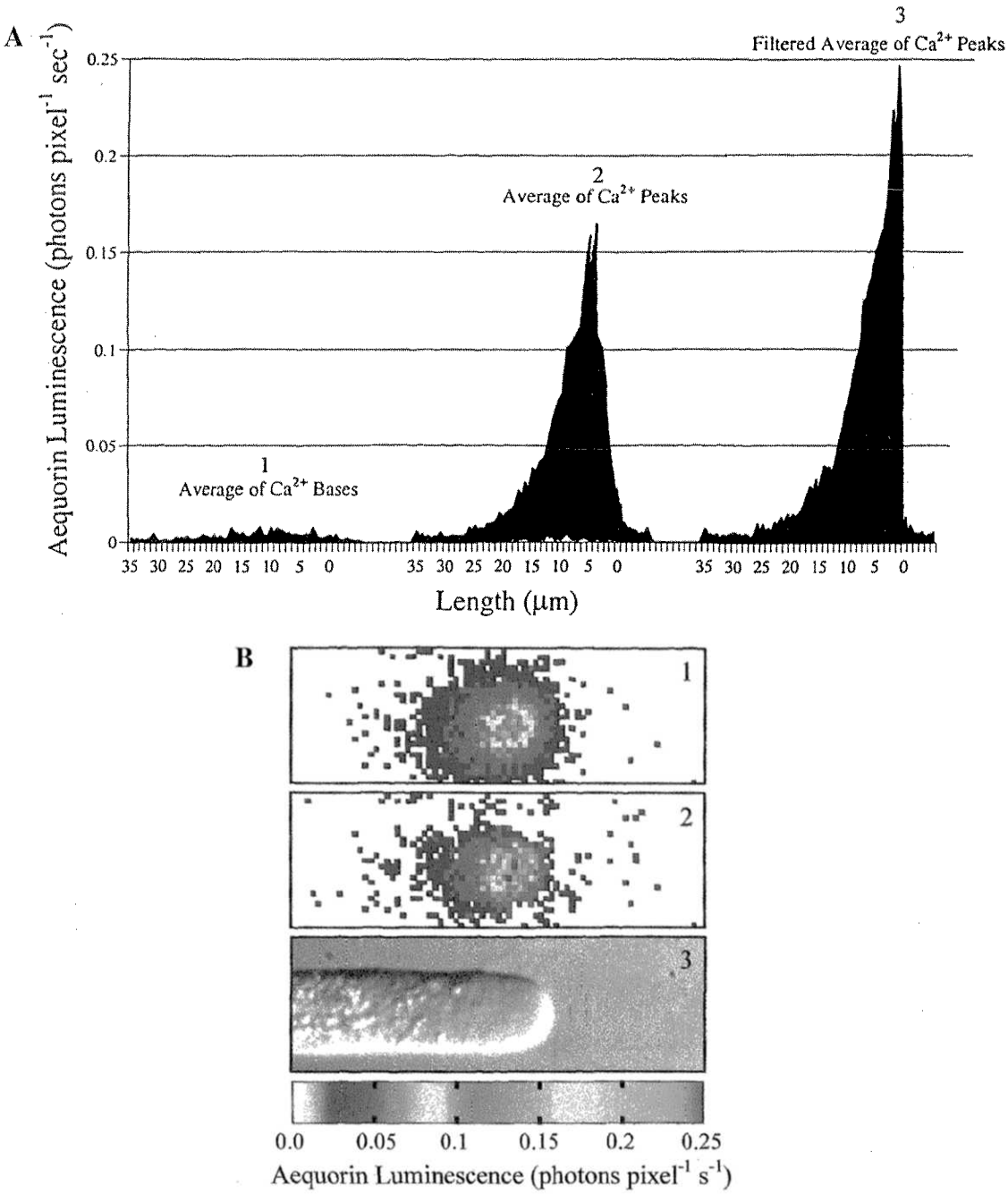

FIG. 6. (A) Intensity profiles of the best-fit alignment and averaging of the light emitted by injected aequorin for a single tube. The tip of the tube is growing toward the right side. (1) A tip-high gradient of light output cannot be distinguished from the alignment of the bases. (2) A sharp peak can be distinguished from the alignment of the Ca^{2+} peaks, which is approximately symmetrical about the highest intensity. Profile (3) shows profile (2) after correcting for scattered light. Profile (3) shows a much steeper increase in light intensity at the tip that declines more gradually down the shaft of the tube. One sees a zone of highest calcium that is only a few micrometers in diameter. (B) Top view of the best-fit alignment of the Ca^{2+} peaks, unfiltered (1) and filtered (2). The tubes are growing toward the right side of the image. The total intensities of the two images are the same. The unfiltered image (1) shows a peak intensity offset just to the right of center, while the filtered image (2) shows the peak intensity much closer to the tip of the tube with gradually declining intensities down the shaft of the tube. Image (3) shows a DIC optics collected image of a growing pollen tube that has been aligned with the aequorin images. Note that as images (1) and (2) are actually the average of a large number of Ca^{2+} oscillations, image (3) is useful only for an approximate comparison.

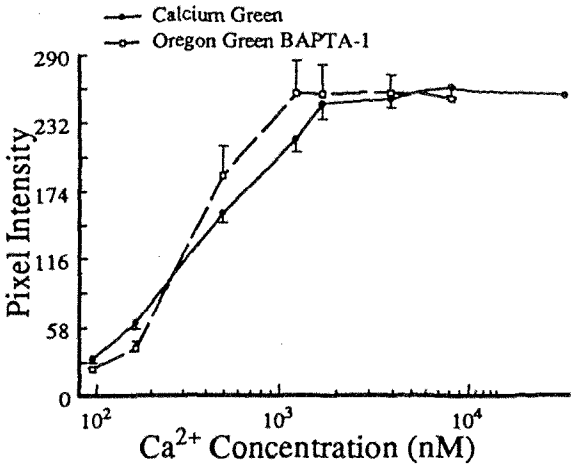

FIG. 7. Calibration curves for Calcium Green/Rhodamine B and Oregon Green Bapta-1/Rhodamine B. Calcium Green and Oregon Green concentrations of 10 and 20 μM were added to an EGTA buffered solution that was designed to mimic the cytosol. The Ca^{2+} concentration was set at specific levels with the aid of a Ca^{2+} buffers computer program. Knowing the concentrations of the components of the calibration solution, we then calculated the final concentration of free Ca^{2+}. The Calcium Green dye appears to saturate around 2 μM while the Oregon Green BAPTA-1 dye saturates around 1 μM.

DISCUSSION

Ca^{2+} Oscillations Lag Growth Oscillations

A careful, high temporal resolution analysis of the relationship between the intracellular Ca^{2+} oscillations and the growth oscillations shows that the Ca^{2+} oscillations lag the growth oscillations by 4.1 $\pm$ 0.2 s. These data are consistent with earlier results showing that the Ca^{2+} oscillations lag those in growth slightly (Messerli and Robinson, 1997). The 5-s resolution with which previous data were acquired was too slow to allow the formation of reliable conclusions. In the present work, we were able to measure growth rates while measuring Ca^{2+} levels with a resolution of 1.5 s, by acquiring video images while counting photons coming from injected aequorin. This enabled us to establish with statistical significance that the increase in Ca^{2+} concentration lags the increase in growth.

This improved temporal resolution depended upon our more accurate timing of the Ca^{2+} peaks as well as the growth peaks. As aequorin's luminescence increases with at least the square of the $[Ca^{2+}]$ (Shimomura, 1995), a doubling of $[Ca^{2+}]$ results in at least a fourfold rise in signal while the same rise in $[Ca^{2+}]$ gives no more than a 25% rise in signal with available dextran-linked fluorescent dyes. This is the main reason that more accurate temporal resolution is possible with aequorin. Moreover, application of newly developed computer vision-based software (Messerli *et al.*, 1999) enables us to measure pollen tube growth to within 1/10 of a pixel with a concomitant improvement in temporal resolution over our earlier use of fluorescent imaging software, which has no less than 1 pixel resolution.

Peak Subsurface Ca^{2+} Levels and Their Significance

The oscillations in tip calcium seen in images such as Fig. 6 are as striking as those seen in purely temporal records (Fig. 5A) and allow an improved estimate of subtip calcium values during these oscillations. The corrected light intensity coming from a 3 $\times$ 3-μm^2 region just under the tip oscillates between values that are 1750- and 170-fold higher than those coming from a region 40 μm behind the tip, whereas fluorescence measurements indicate a Ca^{2+} level of about 236 nM. Assuming a quadratic relationship between light emission and calcium level for aequorin, one infers that the free calcium level in this 3 $\times$ 3-μm^2 subtip region oscillates, on average, between 3 and 10 μM. The higher Ca^{2+} concentration appears to extend over a larger area than shown by the fluorescence-measured gradient shown in Fig. 9B. This is to be expected as the exported aequorin images encompassed 5 s of accumulated light (Fig. 2) so the images are spread over an additional 1.25–2 μm along the direction of growth as the leading edges of the tubes are moving during image acquisition at rates of 0.25–0.4 μm/s. We also think that the fluorescence-measured Ca^{2+} gradients may be reduced in the spatial domain as the fluorescent dyes may collapse the gradient, as indicated by the reduced growth rate of the fluorescent dye imaged tubes. Alternatively the Ca^{2+} gradient may be reduced in fluorescence-imaged cells due to damage by the exciting light or by a nonspecific inhibitory mechanism created by the fluorescent indicator. In any case aequorin appears to be the less damaging method for measuring $[Ca^{2+}]$ so we view the aequorin measurements as the more accurate indicator of the cytosolic $[Ca^{2+}]$. It should be kept in mind that Ca^{2+} uptake by subtip secretory vesicles may well create a gradient such that the levels of free calcium in the critical region just below the plasma membrane are even higher.

These surprisingly high levels of Ca^{2+} at the growing tip restrict the possible Ca^{2+} sensors that may be involved in coupling Ca^{2+} to secretion and growth. Calmodulin and other EF-hand proteins are unlikely to be involved as their Ca^{2+} affinities are too high for them to respond to changes in Ca^{2+} from 3 to 10 μM. Among the viable candidates for the Ca^{2+} sensors in the tip are the C2-domain proteins, of which synaptotagmin is a good example. These proteins have considerably lower Ca^{2+} affinities than the EF-hand proteins and are known to be involved in a wide variety of Ca^{2+}-dependent secretory events (Südhof, 1996).

A Modified Model of Oscillatory Growth

As we have pointed out in the Introduction, like other Ca^{2+}-dependent secretory events, one would expect a rise in subtip Ca^{2+} to precede secretion and thus shortly precede

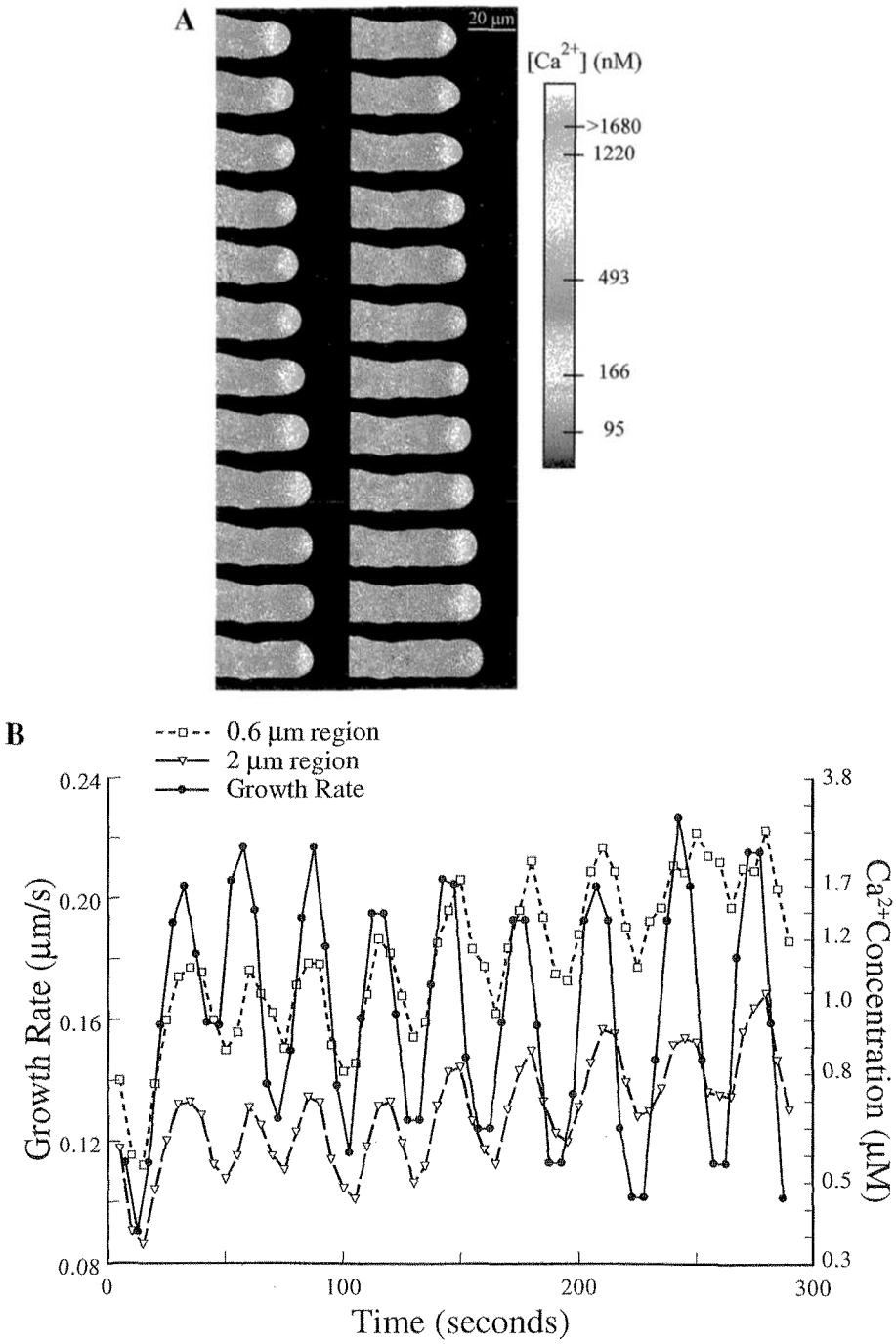

FIG. 8. (A) Intracellular free $[Ca^{2+}]$ in a growing pollen tube, measured via the ratio of Calcium Green dextran to Rhodamine B dextran. Images were acquired 5 s apart. Four Ca^{2+} oscillations are shown in this image train. The tip Ca^{2+} concentration in these images is oscillating between a value above 1.7 μM and below 1.2 μM. The surges in tube growth occur at about the same time as the increases in tip $[Ca^{2+}]$. (B) Ca^{2+} measurements and growth measurements of a different tube collected with fluorescence imaging. Ca^{2+} measurements are shown for two tip regions; a very localized one, 0.6×2.0 μm^2, and a less localized one, 2.0×2.0 μm^2. The $[Ca^{2+}]$ in the smallest region oscillates between 0.9 and 2 μM during this recording. In most cases, the peaks of the Ca^{2+} oscillations lag the peaks of the growth oscillations.

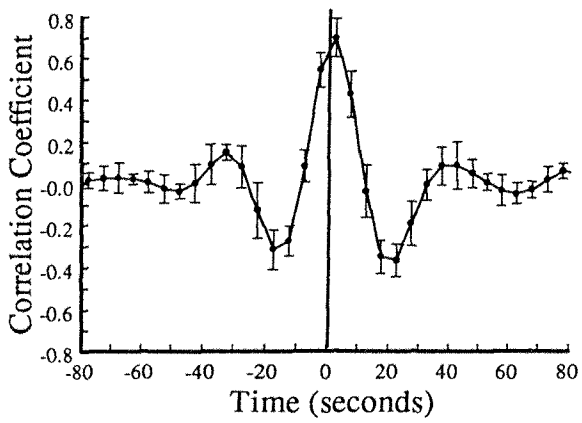

FIG. 9. Correlation analysis plot of the growth rates and tip-localized Ca^{2+} measurements collected through fluorescence imaging. The means ± SE are plotted for the correlation coefficients as the Ca^{2+} concentration curves were shifted with respect to the growth rate curves. The resolution of this method is the same as the resolution of image acquisition, which is 5 s. The highest correlation is when the Ca^{2+} oscillations lag the growth oscillations by 2.5 s.

the release of new membrane components and cell wall materials. Previously proposed models concerning oscillating pollen tube growth have indicated that the rise in intracellular Ca^{2+} and subsequently secretion occurs at the same time as the rise in growth rate (Holdaway-Clarke *et al.*, 1997). The data we present show that the rise in Ca^{2+} and growth rate do not occur at the same time and in fact the growth rate changes occur before the Ca^{2+} changes. Also the relative peak growth rate during the growth oscillations is predictive of the relative magnitude of the peak of the nearest lagging Ca^{2+} oscillation. Our results are more closely supportive of the model proposed by Derksen (1996). However, we think that the osmotic increase proposed in Derksen's model is out of sequence in light of recently published work (Messerli *et al.*, 1999). Also while the sequence of events of Derksen's model is mostly similar to our own, the physiological controls behind Derksen's model were not completely specified. It is for these reasons that we discuss our model, as well as to present testable implications of the model. Table 1 provides data on the main measurable variables reported thus far for oscillatory tube growth, while Fig. 10 shows sinusoidal representations of these together with some key inferred variables that underlie our model, namely, stretch-activated channels, tip turgor pressure, wall plasticity, membrane tension, and membrane potential.

All intracellular ionic changes, extracellular fluxes of specific ions, and net current influx that we have measured are found to oscillate and have amplitudes that are reflective of the preceding growth oscillation. We find that net

TABLE 1
Oscillating Variables Measured during the Growth of Lily Pollen Tubes

Variable	Amplitude	Growth oscillation period (s)	Delay[a] (s)	Phase shift[b] (deg)
$[Ca^{2+}]_i$[c]	3–10 μM	40 ± 3	4 ± 1	n.r.
[d]	0.55–1.2 μM	15–46	−1.6	n.r.
[e]	3–10 μM	39 ± 2	4.1 ± 0.2	38 ± 2
Ca^{2+} influx[d]	5–10 pmol/cm² s	27–33	11	149 ± 4
[f]	38 ± 3 pmol/cm² s	40 ± 3	13.2	123 ± 9
pH_i[g]	0.1–1 pH units (acidic)	n.r.	7.5–12.5	n.r.
[h(1)]	~0.1 pH unit (alkaline)	n.r.	n.r.	n.r.
H^+ influx[f]	489 ± 81 pmol/cm² s	42 ± 4	11	103 ± 9
[h(2)]	0.15–0.4 pmol/cm² s	n.r.	n.r.	n.r.
[i]	~7 pmol/cm² s	34 ± 2	n.r.	n.r.
K^+ influx[f]	688 ± 144 pmol/cm² s	53 ± 5	14	100 ± 11
Net ionic current[g]	0.25–0.45 μA/cm²	n.r.	8 ± 1	n.r.

Note. n.r., not reported.
[a] Delay means time after growth peaks.
[b] Phase shift is the time delay divided by the growth oscillation period multiplied by 360°.
[c] Messerli and Robinson (1997).
[d] Holdaway-Clarke *et al.* (1997).
[e] This paper.
[f] Messerli *et al.* (1999).
[g] Messerli and Robinson (1998). Acidification starts at the tip and travels down the shaft of the tube while decreasing in magnitude.
[h] Feijé *et al.* (1999). (1) An oscillating alkalization behind the clear zone lagging growth oscillations was measured. The extracellular pH was not reported for these experiments. (2) These measurements were collected from a tube growing in a medium with pH 6.5.
[i] Feijó (1998) (Fig. 22.4). Proton influx was reported to vary by 2–3 orders of magnitude among tubes.

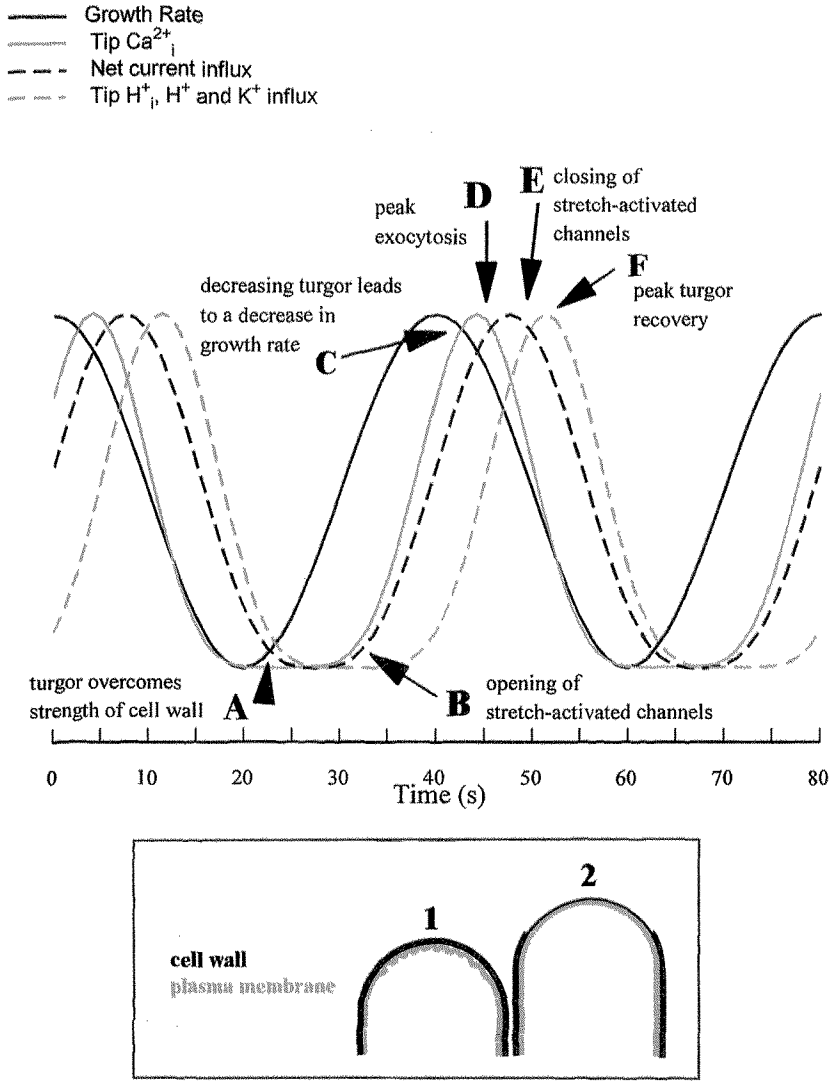

FIG. 10. Model for pollen tube growth. The model shows growth oscillations along with the corresponding increases in the tip $[Ca^{2+}]_i$, net current influx, tip $[H^+]_i$, and H^+ and K^+ influx. Ca^{2+} influx measured with the SERIS probe is not included. At the beginning of a growth surge, the cell membrane is slackened and the cell wall is thickened (inset 1). The state of the membrane and wall is the result of vesicle fusion during or slightly after the previous $[Ca^{2+}]_i$ oscillation. The surge in growth is due to turgor overcoming the strength of the cell wall (A). As little if any secretion occurs at this time, cell expansion both stretches the cell wall and takes the slack out of the membrane (inset 2). Nonspecific stretch-activated channels, which we think lead to the net current influx, are opened (B) in the membrane and allow a small triggering influx of Ca^{2+} which then releases Ca^{2+} from intracellular stores. The increasing growth rate is due to the weakening cell wall as it is thinned by expansion. At the peak of growth, sufficient cell expansion has occurred to reduce turgor, leading to the declining growth rate (C). Also at this time the $[Ca^{2+}]_i$ is reaching its peak, leading to the peak of secretion (D), which occurs at the same time or slightly afterward. The newly secreted cell membrane and cell wall then lead to a slackened membrane and thickened cell wall. This reduces tension in the membrane and leads to the closing of the stretch-activated channels and the reduction in net current influx (E). Following the decrease in growth rate we think that H^+-driven K^+ uptake helps the cell to recover turgor pressure (F) that has dropped during the previous surge in growth. Thus turgor recovers to overcome the strength of the newly added cell wall, creating the beginning of the next growth oscillation.

inward ionic current peaks 7.5 ± 0.5 s after the peak of growth (Messerli and Robinson, 1998). The ions contributing to this net inward current are not known. However, based on the timing of the current, we think that Ca^{2+} influx is at least one component. We assume that the current influx marks the time when nonspecific, stretch-activated cation channels are opened. This occurs as suprathreshold turgor extends the plastic wall placing tension

on the membrane (more below). Opening the channels should immediately reduce the roughly 100-mV membrane potential (Messerli *et al.*, 1999), and oscillations in membrane potential have been observed preliminarily (M.M. and K.R.R., unpublished observation). Stretch-activated channels have been found in at least three other organisms which display tip growth, fungal germ tubes of *Uromyces* (Zhou *et al.*, 1991), hyphae of the water mold *Saprolegnia ferax* (Garrill *et al.*, 1992), and rhizoids of seawater alga *Fucus* (Taylor *et al.*, 1996), and there is evidence that they exist in lily pollen tubes as well (Pierson *et al.*, 1994). In the case of pollen tube growth, we hypothesize that the Ca^{2+} that enters the tube tip (Malhó *et al.*, 1995) raises the cytosolic Ca^{2+} to some critical threshold in order to release Ca^{2+} from intracellular stores. Perhaps the secretory vesicles themselves constitute the intracellular stores (Blondel *et al.*, 1995). In this view, it is mainly this surge in Ca^{2+} that is detected by fluorescent and luminescent indicators. The assumption that the main source of Ca^{2+} is intracellular stores explains the puzzling fact that no influx of Ca^{2+} is detected by the Ca^{2+}-selective self-referencing probe that is temporally correlated with the measured rise in intracellular Ca^{2+} (Holdaway-Clarke *et al.*, 1997; Messerli *et al.*, 1999). Evidence for this view is found in the analysis of the details of the rise in Ca^{2+} as detected by aequorin luminescence (Messerli, 1997, Fig. 2B). There it was shown that the rise in Ca^{2+} is clearly biphasic, with an initial quasi-linear rise followed by an exponential rise in Ca^{2+}; the subsequent fall in Ca^{2+} shows no such biphasic nature. Intracellular Ca^{2+} release also explains how the peak of the tip Ca^{2+} can occur about 3.4 s before the peak of the current influx.

The added membrane, in this model, acts to reduce tension on the membrane and close the stretch-activated channels thus reducing net ionic current entry. We propose that the fusion of vesicles and release of cell wall material during the decrease in growth rate slacken the plasma membrane and produce a relatively thickened cell wall. We imagine that the membrane will look like Fig. 7 in Lancelle *et al.* (1997), in which a fusing vesicle adds to membrane surface area. However, as many more vesicles will be fusing to the plasma membrane, the amount of membrane wrinkling will be more extreme. In Fig. 10, inset 1, we show an exaggerated slackened membrane and a thickened cell wall. It may be difficult to capture the extreme slackened state of the membrane with current techniques as even the least damaging fixation methods have been able to capture only a small number of fusion events (Lancelle *et al.*, 1997) where a dramatically large number of events are expected to occur. The state of the membrane may be studied more closely in real time with fluorescent membrane dyes that desaturate upon addition of new membrane. An interesting indication that wall thickness does in fact oscillate is provided by observations of growing *Gasteria* pollen tubes that show a detectable undulation of wall thickness during oscillating tube growth (Plyushch *et al.*, 1995). Undulations in wall thickness have also been induced when pollen tubes were forced to grow in an oscillating fashion (Li *et al.*, 1996).

Due to the surge in growth and the resultant increase in cytoplasmic volume, the turgor will have decreased. The turgor is partially restored, we think, by H^+-driven K^+ uptake (Messerli *et al.*, 1999). It is the generation of a critical threshold of turgor that overcomes the cell wall strength necessary to promote growth. After turgor has reached a critical threshold, the thickened cell wall yields, leading to another growth surge. As little secretion occurs at this time, any further elongation will stretch the existing cell wall and take the slack out of the membrane, thus tensing the membrane (Fig. 10, inset 2). Tension in the membrane then opens stretch-activated channels leading to the triggering amount of Ca^{2+} that releases Ca^{2+} from intracellular stores. Oscillations in turgor pressure are a key component of our model. Benkert *et al.* (1997) failed to detect any such oscillations. This is expected, as most of the tubes that they examined were not long enough to be growing in an oscillating manner. It has been reported that lily pollen tubes begin showing oscillating growth (Pierson *et al.*, 1996) or oscillating current influx (Weisenseel *et al.*, 1975) when the tubes are greater than 700 and 1000 μm, respectively, and oscillating tip $[Ca^{2+}]_i$ (Messerli and Robinson, 1997) 2.5 h after the tubes have been in culture, when they are approximately 800 μm long. Additionally the probe used by Benkert *et al.* (1997) was adequate for measuring average cell turgor but appears not to have sufficient sensitivity or temporal resolution for measuring the turgor oscillations. Pressure of 4 kPa was sufficient to shift calcium-permeable stretch-activated channels of *Uromyces* germ tubes (Zhou *et al.*, 1991) from their 0% to their 100% open probability state and to open Ca^{2+}-permeable stretch-activated channels in *Saprolegnia* hyphae (Garrill *et al.*, 1992). This value is less than the sensitivity resolution of the turgor probe used by Benkert *et al.* (1997), which is only 5 kPa. Furthermore, if channels with similar gating characteristics existed in the approximately twofold larger diameter pollen tubes the pressure needed to place the same tension on the membrane to open these channels would decrease by half to 2 kPa. (Tension is directly proportional to pressure and diameter of a spherical thin walled vessel.) Also, the method of pressure measurement, manual adjustment of the oil/cytosol interface, may not have been adequate to achieve the necessary temporal resolution of 1–2 s.

An alternative hypothesis for the generation of the growth oscillations involves constant turgor pressure in conjunction with oscillations in the rigidity of the cell wall. It was proposed that cell wall acidification would weaken the wall and lead to a surge in growth, then addition of Ca^{2+} to the newly released cell wall would strengthen the wall and reduce the rate of growth (Holdaway-Clarke *et al.*, 1997). While Ca^{2+} may increase the rigidity of polymerizing pectin and may be a component of reducing the growth rate, tip wall acidification does not appear to occur in lily pollen tubes. Tip cell wall acidification has been demonstrated with a pH-sensitive fluorescent dye and appears to be necessary for *Arabidopsis* root hair growth (Bibikova *et al.*,

TABLE 2
Lily Pollen Tube Growth Speeds *in Situ* and *in Vitro*

Speed (μm/s)		
In situ	*In vitro*	Reference
0.27–0.43		1914[a]
0.23		1995[b]
	0.25	1996[c]
	0.17–0.18	1997[d]
	0.18–0.20	1997[e]
	0.24	This paper

[a] Togukawa (1914).
[b] Jauh and Lord (1995) for the first 2 cm of stylar growth.
[c] Pierson *et al.* (1996).
[d] Messerli and Robinson (1997).
[e] Holdaway-Clarke *et al.* (1997) under regular medium conditions.

1998). However, quite a different picture has emerged for pollen tubes. Efflux of H^+ has been proposed to acidify the tip cell wall of the root hairs but the opposite, H^+ influx, has been measured at the tips of growing lily pollen tubes (Feijó *et al.*, 1999; Messerli *et al.*, 1999), suggesting, if anything, that the immediately adjacent tip cell wall is less acidic than the bath medium. The measured pH at the tip is greater by up to 0.03 pH units (Messerli *et al.*, 1999) and is never found to be more acidic than the bath medium. In summary the timing of the $[Ca^{2+}]$ oscillations and growth oscillations are similar to those of Derksen's (1996) model while not consistent with the models proposed by Holdaway-Clarke *et al.* (1997). We, however, have suggested physiological mechanisms for the generation of the growth and Ca^{2+} oscillations that are fundamentally different from Derksen's model.

In vitro studies of pollen tube growth have yielded much information at the biological and physiological levels. However, serious uncertainties inevitably arise at the whole system level at which observations of isolated pollen tube growth reveal only possibilities. One of the few aspects of pollen tube growth that has been measured both within the flower and *in vitro* is the elongation rate. Table 2 critically compiles data on stylar rates, data that incorporate *in situ* growth rates from *L. longiflorum*, and compares them with recent measurements of *L. longiflorum in vitro* rates in optimal medium. While this compilation is not exhaustive, it shows that such *in vitro* rates in *L. longiflorum* are practically the same as stylar rates. This then raises the question of whether stylar growth is also oscillatory. A first indication that stylar growth is indeed oscillatory was provided by a study by Li *et al.* (1992) on tobacco pollen. They observed periodic bands of arabinogalactan epitopes within tubes that were growing semi-*in vivo*, i.e., backward, toward a cut style's surface but still within the style. This banding was quite similar to that seen by them *in vitro*. Advances in imaging may soon make it feasible to answer that question more confidently. One could imagine following a tube's progress within a living style by labeling its advancing tip with aequorins or with GFPs.

ACKNOWLEDGMENTS

We thank Theresa Kirk of Purdue University's Horticulture Department for harvesting the pollen for this work; Dr. Osamu Shimomura at the Marine Biological Laboratory (Woods Hole, MA) and Dr. S. Inouye, Chisso Corp. (Yokohama, Japan), for providing the recombinant aequorin; Theodore Van Rijk, Bruce Fuller, and Thomas Keating for their contributions to the video/photon measuring system; J. Paul Robinson and Huw S. Kruger Gray of the Purdue Cytometry Laboratory for their help with the scanning confocal imaging. This research was funded by NSF Grant IBN 9600568, NIH Grant P41RR013905, a Purdue Research Foundation Fellowship, and a Journal of Cell Science Travel Fellowship awarded to M. A. Messerli.

REFERENCES

Avery, J., Reinhard, J., and Edwardson, J. M. (1999). Reconstitution of regulated exocytosis in cell-free systems: A critical appraisal. *Annu. Rev. Physiol.* **61,** 777–807.

Baram, D., Linial, M., Mekori, Y. A., and Sagi-Eisenberg, R. (1998). Cutting edge: Ca^{2+}-dependent exocytosis in mast cells is stimulated by the Ca^{2+} sensor, synaptotagmin I. *J. Immunol.* **161,** 5120–5123.

Benkert, R., Obermeyer, G., and Bentrup, F.-H. (1997). The turgor pressure of growing lily pollen tubes. *Protoplasma* **198,** 1–8.

Bibikova, T. N., Jacob, T., Dahse, I., and Gilroy, S. (1998). Localized changes in apoplastic and cytoplasmic pH are associated with root hair development in *Arabidopsis thaliana*. *Development* **125,** 2925–2934.

Blinks, J. R. (1989). Use of calcium-regulated photoproteins as intracellular Ca^{2+} indicators. *Methods Enzymol.* **172,** 164–203.

Blondel, O., Bell, G. I., and Seino, S. (1995). Inositol 1,4,5-trisphosphate receptors, secretory granules and secretion in endocrine and neuroendocrine cells. *Trends Neurosci.* **18,** 157–161.

Chow, R. H., Jürgen, K., and Neher, E. (1994). Time course of Ca^{2+} concentration triggering exocytosis in neuroendocrine cells. *Proc. Natl. Acad. Sci. USA* **91,** 12765–12769.

Derksen, J. (1996). Pollen tubes: A model system for plant cell growth. *Bot. Acta* **109,** 341–345.

Feijó, J. A. (1998). The pollen tube oscillator: Towards a molecular mechanism of tip growth? *In* "Fertilization in Higher Plants" (M. Cresti, G. Cai, and A. Moscatelli, Eds.), pp. 317–336. Springer-Verlag, Berlin/New York.

Feijó, J. A., Sainhas, J., Hackett, G. R., Kunkel, J. G., and Hepler, P. K. (1999). Growing pollen tubes possess a constitutive alkaline band in the clear zone and a growth-dependent acidic tip. *J. Cell Biol.* **144,** 483–496.

Franklin-Tong, V. E. (1999). Signaling and the modulation of pollen tube growth. *Plant Cell* **11,** 727–738.

Garrill, A., Lew, R. R., and Heath, I. B. (1992). Stretch-activated Ca^{2+} and Ca^{2+}-activated K^+ channels in the hyphal tip plasma membrane of the oomycete *Saprolegnia ferax*. *J. Cell Sci.* **101,** 721–730.

Holdaway-Clarke, T. L., Feijó, J. A., Hackett, G. R., Kunkel, J. G., and Hepler, P. K. (1997). Pollen tube growth and the intracellular cytosolic calcium gradient oscillate in phase while extracellular calcium influx is delayed. *Plant Cell* **9,** 1999–2010.

Jauh, G. Y., and Lord, E. M. (1995). Movement of the tube cell in the lily style in the absence of the pollen grain and the spent pollen tube. *Sex. Plant Reprod.* **8,** 168–172.

Lancelle, S. A., Cresti, M., and Hepler, P. K. (1997). Growth inhibition and recovery in freeze-substituted *Lilium longiflorum* pollen tubes: Structural effects of caffeine. *Protoplasma* **196,** 21–33.

Li, Y. Q., Brunn, L., Pierson, E. S., and Cresti, M. (1992). Periodic deposition of arabinogalactan epitopes in the cell wall of pollen tubes of *Nicotiana tabacum* L. *Planta* **188,** 532–538.

Li, Y.-Q., Zhang, H.-Q., Pierson, E. S., Huang, F.-Y., Linskens, H. F., Hepler, P. K., and Cresti, M. (1996). Enforced growth-rate fluctuation causes pectin ring formation in the cell wall of *Lilium longiflorum* pollen tubes. *Planta* **200,** 41–49.

Malhó, R., Read, N. D., Trewavas, A. J., and Pais, M. S. (1995). Calcium channel activity during pollen tube growth and reorientation. *Plant Cell* **7,** 1173–1184.

Messerli, M., and Robinson, K. R. (1997). Tip localized Ca^{2+} pulses are coincident with peak pulsatile growth rates in pollen tubes of *Lilium longiflorum*. *J. Cell Sci.* **110,** 1269–1278.

Messerli, M. A., Danuser, G., and Robinson, K. R. (1999). Pulsatile influxes of H^+, K^+, and Ca^{2+} lag growth pulses of *Lilium longiflorum* pollen tubes. *J. Cell Sci.* **112,** 1497–1509.

Messerli, M. A., and Robinson, K. R. (1998). Cytoplasmic acidification and current influx follow growth pulses of *Lilium longiflorum* pollen tubes. *Plant J.* **16,** 87–91.

Miller, A. L., Karplus, E., and Jaffe, L. F. (1994). Imaging $[Ca^{2+}]_i$ with aequorin using a photon imaging detector. *In* "Methods in Cell Biology: A Practical Guide to the Study of Calcium in Living Cells" (R. Nuccitelli, Ed.), Vol. 40, pp. 305–338. Academic Press, San Diego.

Miller, D. D., Callaham, D. A., Gross, D. J., and Hepler, P. K. (1992). Free Ca^{2+} gradient in growing pollen tubes of *Lilium*. *J. Cell Sci.* **101,** 7–12.

Pierson, E. S., Li, Y. Q., Zhang, H. Q., Willemse, M. T. M., Linskens, H. F., and Cresti, M. (1995). Pulsatory growth of pollen tubes: Investigation of a possible relationship with the periodic distribution of cell wall components. *Acta Bot. Neerl.* **44,** 121–128.

Pierson, E. S., Miller, D. D., Callaham, D. A., Shipley, N. M., Rivers, B. A., and Hepler, P. K. (1994). Pollen tube growth is coupled to the extracellular calcium ion flux and the intracellular calcium gradient: Effect of BAPTA-type buffers and hypertonic medium. *Plant Cell* **6,** 1815–1828.

Pierson, E. S., Miller, D. D., Callaham, D. A., van Aken, J., Hackett, G., and Hepler, P. K. (1996). Tip-localized calcium entry fluctuates during pollen tube growth. *Dev. Biol.* **174,** 160–173.

Plyushch, T. A., Willemse, M. T. M., Franssen-Verheijen, M. A. W., and Reinders, M. C. (1995). Structural aspects of *in vitro* pollen tube growth and micropylar penetration in *Gasteria verrucosa* (Mill.) H. Duval and *Lilium longiflorum* Thunb. *Protoplasma* **187,** 13–21.

Rathore, K. S., Cork, R. J., and Robinson, K. R. (1991). A cytoplasmic gradient of Ca^{2+} is correlated with the growth of lily pollen tubes. *Dev. Biol.* **148,** 612–619.

Sabatini, B. L., and Regehr, W. G. (1996). Timing of neurotransmission at fast synapses in the mammalian brain. *Nature* **384,** 170–172.

Shimomura, O. (1995). Luminescence of aequorin is triggered by the binding of two calcium ions. *Biochem. Biophys. Res. Commun.* **211,** 359–363.

Südhof, T. C. a. R. (1996). Synaptotagmins: C2-domain proteins that regulate membrane traffic. *Neuron* **17,** 379–388.

Tang, X.-w., Liu, G.-q., Yang, Y., Zheng, W.-l., Wu, B.-c., and Nie, D.-t. (1992). Quantitative measurement of pollen tube growth and particle movement. *Acta Bot. Sin.* **34,** 893–898.

Taylor, A. R., Manison, N. F. H., Fernandez, C., Wood, J., and Brownlee, C. (1996). Spatial organization of calcium signaling involved in cell volume control in the *Fucus* rhizoid. *Plant Cell* **8,** 2015–2031.

Togukawa, Y. (1914). Zur physiologie des pollens. *J. Coll. Sci. Tokyo Imp. Univ.* **35,** Art. 8.

Weisenseel, M. H., Nuccitelli, R., and Jaffe, L. F. (1975). Large electrical currents traverse growing pollen tubes. *J. Cell Biol.* **66,** 556–567.

Zhou, X.-L., Stumpf, M. A., Hoch, H. C., and Kung, C. (1991). A mechanosensitive channel in whole cells and in membrane patches of the fungus *Uromyces*. *Science* **253,** 1415–1417.

Zorec, R., and Tester, M. (1992). Cytoplasmic calcium stimulates exocytosis in a plant secretory cell. *Biophys. J.* **63,** 864–867.

Received for publication January 10, 2000
Revised March 15, 2000
Accepted March 15, 2000